PCCP

PEGylation within a Confined Hydrophobic Cavity of a Protein

Journal:	*Physical Chemistry Chemical Physics*
Manuscript ID	CP-ART-08-2019-004387.R1
Article Type:	Paper
Date Submitted by the Author:	25-Oct-2019

Complete List of Authors:	Munasinghe, Aravinda; University of Florida, Department of Chemistry Mathavan, Akshay; University of Florida, Department of Chemistry Mathavan, Akash; University of Florida, Department of Chemistry Lin, Ping; University of Florida, Chemistry Coray, Colina; University of Florida, Department of Chemistry

PEGylation within a Confined Hydrophobic Cavity of a Protein

Aravinda Munasinghe[1,2,3,#], Akshay Mathavan[1,2,4,#], Akash Mathavan[1,2,4], Ping Lin[1,2,3] and Coray M. Colina[1,2,3,5,*]

[1]Department of Chemistry, [2]George & Josephine Butler Polymer Research Laboratory, [3]Center for Macromolecular Science & Engineering, [4]Department of Biomedical Engineering, and [5]Department of Materials Science and Engineering, University of Florida, Gainesville, Florida 32611, United States

[#]Aravinda Munasinghe and Akshay Mathavan contributed equally to this work

[*]Corresponding author: Email: colina@chem.ufl.edu, Phone: +1 (352) 294-3488

Abstract

The conjugation of polyethylene glycol (PEG) to proteins, known as PEGylation, has increasingly been employed to expand the efficacy of therapeutic drugs. Recently, research has emphasized the effect of the conjugation site on protein-polymer interactions. In this study, we performed atomistic molecular dynamics (MD) simulations of lysine 116 PEGylated bovine serum albumin (BSA) to illustrate how conjugation near a hydrophobic pocket affects the conjugate's dynamics and observed altered low mode vibrations in the protein. MD simulations were performed for a total of 1.5 μs for each PEG chain molecular mass from 2 to 20 kDa. Analysis of preferential PEG-BSA interactions showed that polymer behavior was also affected as proximity to the attractive protein surface patches promoted interactions in small (2 kDa) PEG chains, while the confined environment of the conjugation site reduced the expected BSA surface coverage when the polymer molecular mass increased to 10 kDa. This thorough analysis of PEG-BSA interactions and polymer dynamics increases the molecular understanding of site-specific PEGylation and enhances the use of protein-polymer conjugates as therapeutics.

Keywords

Atomistic molecular dynamics, bioconjugate, bovine serum albumin, domain motions, PEGylation

Introduction

The emergence of protein therapeutics has presented new opportunities in treating diseases but intrinsic limitations such as immunogenicity, instability, and susceptibility to renal clearance and proteolysis may still persist.[1–3] This has prompted growing interest in "polymer therapeutics", where covalent linkage of polymers to proteins creates versatile therapeutic agents that can be synthesized with a focus on any number of protective effects.[4–6] One of the most effective strategies involves conjugation of polyethylene glycol (PEG) to a protein, known as PEGylation.[7] The PEG polymer is biocompatible, soluble in both organic and aqueous environments, and highly hydrated such that it can shield proteins from clearance and immunoactivity.[8–12] Thus, PEGylation helps improve pharmaceutical efficacy; however, its effectiveness is dependent on the tailored architecture of the protein-polymer conjugate, including the length of the polymer, the site of conjugation, and the number of attached polymers.

The importance of characterizing PEG chains arises from the fact that their configuration remains a key factor in the utility of protein-polymer conjugates. Two prevailing models used to designate polymer conformations are the shroud model, where the PEG chain wraps around the protein and may generate a shielding effect, and the dumbbell model, where the PEG chain exists as a random coil and dangles away from the protein.[7,11,13,14]

Varying relationships between the size and shape of PEG polymers[15–22] have been proposed, including an observed transition in PEG shape from the dumbbell to the shroud conformation as a function of increasing PEG chain molecular mass (MM) as well as conflicting reports of observed shroud or dumbbell conformations in high MM (20 kDa) PEG chains.[20–22] The complicated nature associated with elucidating PEG chain conformations and their effects on conjugates has been recently stressed in work by Vernet and co-workers.[23]

Resolving PEG chain conformations within conjugates remains a difficult task as the large and flexible nature of the polymer limits the use of protein crystallography for determination of structure and light scattering methods can involve extensive parameter fitting.[24,25] Cattani et al. crystallized a 5 kDa PEGylated plastocyanin protein and their work showed the “dumbbell” model was favored while reporting that electron density was not observed for PEG due to its disordered nature within the porous region.[25] Computational studies have been increasingly utilized to understand molecular mechanisms involved in PEGylation and have shown predictive potential, both of which are necessary for the manufacturing of new conjugate systems.[26–32] In a recent study, we performed atomistic molecular dynamics (MD) simulations of N-terminal conjugated PEG-BSA (bovine serum albumin) using 2, 5, 10, and 20 kDa PEG MMs.[33] Human serum albumin (HSA) is the most prevalent circulatory protein in humans, serving as a carrier protein for fatty acids, thyroid hormones, and steroids, and thus is a target for PEGylated therapeutics studies.[34–36] BSA is structurally and functionally analogous to HSA, consisting of three domains that form a “heart” shaped globular structure.[37] Therefore, the protein has been a model compound and subject of several experimental and computational works examining the effects of PEGylation.[7,15,16,38] Due to the availability of experimental and simulation data on PEGylated BSA, the protein was selected to explore the effects of PEGylation in our previous work, and results not only showed a similar increase in PEG’s affinity for the protein surface as a function of PEG MM, but also revealed preferential PEG-BSA interactions. It was seen that the polymer formed more contacts with domains I and III of the BSA; furthermore, PEG tended to coordinate more around lysine residues of the protein which were surrounded by hydrophobic residues, highlighting how the underlying chemical nature of the environment affected the PEG chain’s behavior.

While many works, both experimental and computational, have investigated PEG chain behavior in regard to shape and polymer length, only few studies have also emphasized the importance of the conjugation site and their effects toward the native dynamics of the protein.[18,27,39–42] Recent work by Ramberg et al. on hexavalent lectin extensively explored how the degree of conjugation affects resulting protein activity through experimental and computational modelling. Their work proposed that reduced activity was related to the PEG chain sterically hindering substrate accessibility.[43] Mu et al.[27] studied 5 and 20 kDa PEGylated Staphylokinase (Sak) with site-specific conjugation at the N-terminus and C-terminus. Results from sedimentation velocity analysis and solvent accessible surface

area (SASA) calculations showed that PEGylation sites affected the hydrodynamic shape of the conjugate, an important factor in retention time. Additionally, docking analyses on Sak-micro-plg complexes, composed of PEGylated Sak and its receptor plasminogen (represented by micro-plasminogen), revealed higher binding affinity with C-terminally PEGylated Saks than N-terminally PEGylated Saks. Work by Kim et al.[40] on Exendin-4 PEGylated at the N-terminus, C-terminus, and nonspecific lysine residues similarly showed improved receptor binding and blood circulation half-life in C-terminally PEGylated conjugates. Studies have shown that PEGylation of proteins near their bioactive sites can lead to reduced activity of the conjugates whereas site-specific PEGylation further from such regions reduces loss of efficacy.[44–46] While this seems sensible, one must also consider effects of and to the local environment of the conjugation site, such as crowding, induced internal domain motions and the chemical composition of the accessible protein surface. Domain motion can be directly related to protein function, such as those in ligand-induced conformational changes. In serum albumins, such as HSA, domain motions have been analyzed with regard to structural changes upon fatty acid binding, where a study by Fujiwara et al.[47] suggested an inherent link between motions of domain I and III and the binding of myristates and the resulting increase in radius of gyration of the protein. Biswas and coworkers[48] investigated the behavior of HSA in crowded milieu by considering variations in interdomain distances and observed both correlated and anti-correlated domain motions, varying by crowding agent.

PEG has recently been employed as a macromolecular crowding agent in several studies.[49,50] Thus, it is reasonable to expect that the polymer may cause similar changes to domain motions. A study by Ciepluch et al.[28] investigating the effects of PEGylation on phosphoglycerate kinase focused on domain dynamics related to closing of the protein cleft. Evaluation of motional amplitudes showed that PEGylation did not significantly influence internal domain motions; instead, the polymer was found to behave as an entropic spring that pushes and pulls the entire protein as a separate, dumbbell-like segment. However, coarse grained simulations of PEGylated glutamate dehydrogenase by Zaghmi et al.[51] investigated mechanisms of activity loss other than the often cited coverage of the protein's surface to instead show protein dynamics were directly affected. The authors employed normal mode analyses, where normal modes were calculated and ranked according to amplitudes of motion, to illustrate reduction of the lowest ranking mode and dampened motions related to closure of the catalytic cleft upon PEGylation. Furthermore, dampened large-scale motions were attributed to adherence or interactions between the PEG polymer and the protein surface, although instances of dumbbell-like PEG chains reducing motions through a "parachute effect"[17] were also seen. Clearly, the exact mechanisms by which the site of PEGylation influences both protein-PEG interactions and local changes in the protein remain unresolved and a greater molecular understanding is necessary for utilizing PEGylated products in many applications, such as acting as phase transfer agents.[52–54]

In this work, atomistic MD simulations of lysine 116 (K116) conjugated PEG-BSA systems were performed with 2, 5, 10, and 20 kDa linear PEG chains to exemplify the effects of the conjugation site on PEG behavior across varying PEG chain lengths. Comparisons with results from previous simulation work on N-terminal conjugated BSA systems were performed as N-terminal conjugation is readily accessible experimentally and is often modelled computationally. K116 is situated in a surface accessible loop structure between domains I and III of the BSA and can be readily conjugated to PEG via a linker. Additionally, the conjugation site maintains close proximity to binding sites within BSA (e.g., drug binding Sudlow sites[55,56]). Therefore, our work not only provides insight on patterns of interaction between PEG and BSA at the atomistic scale across conjugation sites, but also shows how the environment of a conjugation site turns PEG into a local crowding agent around a prominent binding site (K116), which in turn can be used to evaluate domain motions.

Methodology

Results for 6 μs of total accumulated simulation time using the NAMD 2.13 software package[57] are presented for K116 PEGylated BSA systems. The initial structure for the BSA protein was generated from crystallographic information available in the RCSB Protein Data Bank (entry 4F5S).[58] The protonation state of each amino acid residue of the BSA was assigned through the AmberTools16 Reduce code.[59] Protonation of residues, including histidine, was conducted at pH 7 to mimic biological conditions. PEG polymers were assembled using 45, 113, 227, and 454 monomer units to achieve MMs of 2, 5, 10, and 20 kDa, respectively. This assembly was implemented through the PySimm software's force field assisted linear self-avoiding random walk method.[60] Because the polymer is not naturally reactive to covalent linkage to a protein by itself, a carbamate linker was used to link PEG to K116 of the BSA (**Figure S1**), as is done experimentally.[61] The protein, the PEG polymer, and the carbamate linker were modelled using the CHARMM C36m force field, the CHARMM ether force field, and the CGenFF force field, respectively.[62–64] Moreover, atom typing and assignment of parameters and charges by analogy for the linker were derived using the CGenFF web server developed by Vanommeslaeghe and coworkers.[65,66] The psfgen tool within the Visual Molecular Dynamics (VMD) software[67] was used to construct topology files of the protein-polymer conjugate systems.

Due to the flexibility of the PEG chain, the conformational space probed by the polymer is complex, particularly for high MM PEG chains. To obtain adequate sampling of the BSA's surface by the PEG chain, ten different initial configurations of the grafted PEG (PEG chain conjugated to the protein) were generated for each PEG chain by distributing initial polymer orientations uniformly across the protein's accessible surface (**Figure S2**). Results of our MD simulations were compared against free (no PEGylation) BSA (500 ns), as well as for the ten N-terminal PEGylated BSA systems for each MM (150 ns each) and free PEG polymers (300 ns each) studied in our previous works for comparison of

protein-polymer dynamics.[33,68] While an oxime linker was used in the N-terminal PEGylated BSA systems, both the oxime linker and the carbamate linker utilized in this work are short, neutral molecules. The generated K116 PEGylated BSA structures were solvated with explicit TIP3P[69,70] water, as adapted in NAMD, in a cubical box with a minimum buffering distance of 14 Å from any edge of the conjugate to any edge of the box. Since periodic boundary conditions were used, the minimum distance between images was tracked to ensure no artifacts were present due to interactions between images. Thus, a 14 Å buffering distance was found to be adequate. Systems were neutralized by adding Na^+ and Cl^- ions, simulating physiological concentrations of 0.15 M. Resulting simulation system sizes for each of the ten simulations, designated by "sim ID", for each PEG MM are reported in **Table S1**.

MD simulations were conducted using the NAMD program. First, energy minimization was performed in two steps: 1) protein backbone atoms were restrained to initial coordinates using a harmonic potential with a scaled force constant of 500.0 kCal/mol and then 2) the entire system was relaxed with all restraints removed. Each step utilized 10,000 steps of the conjugate gradient method, with a 10 Å switching distance and 12 Å cutoff for all nonbonded interactions. The Particle Mesh Ewald algorithm was used for long range electrostatic interactions.[71] Each system was then heated from 0 to 300 K while protein atoms were restrained with a harmonic potential with a scaled force constant of 10.0 kCal/mol. Heating was conducted in 50 K increments and 20 ps intervals in the NVT ensemble, followed by an additional 500 ps of simulation. Then, NPT simulations were performed at 1 bar and 300 K, maintained using the Langevin thermostat and a collision frequency of 1.0 ps^{-1}. The SETTLE algorithm was applied throughout all MD simulations to place constraints on any bond lengths containing hydrogen atoms, permitting a time step of 2 fs.[72] Thus, MD simulations were performed for a total of 1.5 μs (10 simulations of 150 ns) for each PEG chain MM. The resulting trajectories were analyzed using the VMD software[67], the ProDy dynamics analysis package[73,74], and in-house python and tcl scripts.

Results and discussion

Structure and Dynamics of Grafted PEG Chains

Resolving the specific conformation of PEG in bioconjugates remains a challenging but important task as the polymer's shape may directly impact pharmaceutical properties of protein-polymer therapeutics. As mentioned earlier, two dominant models used to characterize PEG shape include the shroud model and the dumbbell model. Relationships between PEG size and shape have been proposed. Numerous studies have indicated a transition from dumbbell-like to shroud-like conformation upon increasing PEG MM but a correlation as a function of MM has not been elucidated.[20–

[22,31,32] This transition may be affected by the local environment of the PEG-protein grafting site.

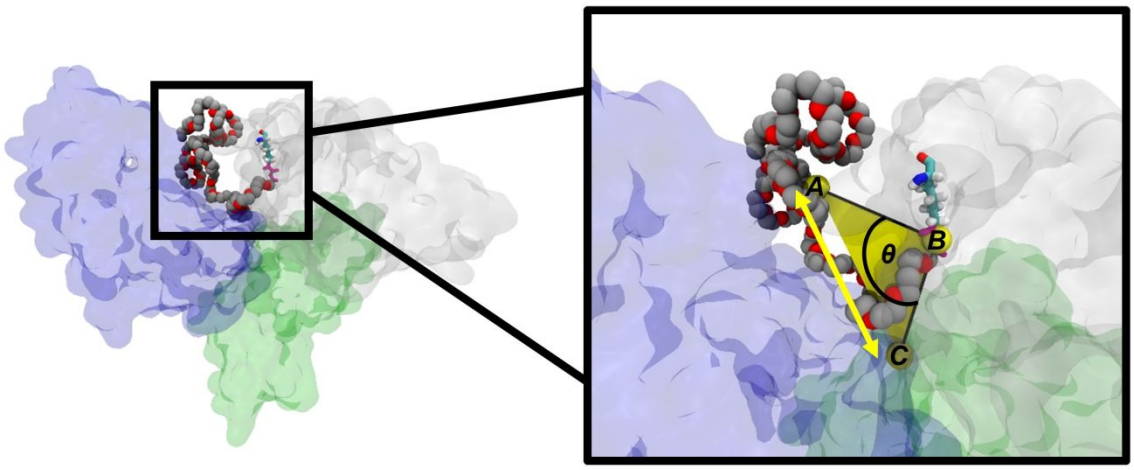

Figure 1. Visualization of a 2 kDa K116 PEGylated BSA conjugate. The BSA is partitioned into domain I (gray), domain II (green), and domain III (blue). PEG oxygen and carbon atoms are shown as red and gray van der Waals spheres, respectively. K116 and the carbamate linker (pink) are presented in licorice model representations. Centers of mass of the PEG chain, carbamate linker, and BSA are shown on the right as yellow van der Waals spheres (labeled A, B, and C, respectively). The angle between the centers of mass (∠ABC) is denoted *θ*. The distance between the centers of mass of protein and PEG ($D_{PEG,\,BSA}^{COM}$) is depicted by the yellow arrow (distance between A and C).

PEG chains' shapes have been experimentally estimated through comparison of individual PEG and protein geometries to that of the conjugate[22,75]. For instance, the hydrodynamic diameters of free protein and free PEG can be compared to the total value for the conjugate, and a rough equivalence implies a dumbbell-like conformation for the PEG chain. In MD simulations of PEGylated systems, the conformation of PEG can be approximated through measurement of several distances and radius of gyration (R_g) values: comparison of the sum (referred to as R_s) of the R_g of free protein, found to be 27.5 ± 0.3 Å for BSA, and R_g of free PEG to the distance between the centers of mass of protein and PEG (referred to as $D_{PEG,\,BSA}^{COM}$) in the conjugate. **Figure 1** illustrates the $D_{PEG,\,BSA}^{COM}$ measurement (yellow arrow). When the R_s is less than or equal to the $D_{PEG,\,BSA}^{COM}$ the dumbbell-like conformation is predicted to be favorable, whereas the shroud-like conformation is presumed to be favorable when R_s is greater than the $D_{PEG,\,BSA}^{COM}$. However, results from applying the above geometrical analysis to K116 PEGylated systems may be biased toward indicating shroud-like conformations as the conjugation site is located within the volume defined by free BSA R_g; therefore, a correction factor was calculated, as discussed in **Figure S3**. Briefly, the distance between the center of mass of the BSA and the Cα atom of K116 was measured and shown to be 24.0 ± 1.6 Å. A correction factor (3.5 Å) was defined as the difference between the R_g of free BSA and the previous value and added to all final measured $D_{PEG,BSA}^{COM}$ averages. Additionally, direct comparison between R_g of free PEG to that of grafted PEG also provided insight into PEG shape. To

characterize the shape of PEG in the K116 PEGylated BSA systems, the radii of gyration and $D^{COM}_{PEG,\,BSA}$ were measured and are reported in **Table 1**. For each PEG MM, the last 150 ns of each trajectory for the ten systems was used to calculate average values for R_g and $D^{COM}_{PEG,\,BSA}$ measurements. Additionally, the percentage of time during which the grafted PEG chains maintained a shroud-like conformation was calculated from the aggregated 1.5 μs of data for each PEG MM (ten systems of 150 ns each).

Table 1. Radius of gyration for free PEG, grafted PEG, sum of free PEG and free protein (R_s), and distance between centers of mass of PEG and BSA ($D^{COM}_{PEG,BSA}$) in conjugates. Fraction of time in which PEG assumed a shroud-like conformation ($R_s > D^{COM}_{PEG,BSA}$) in K116 and N-terminal PEGylated systems is also reported. Values in radius of gyration and $D^{COM}_{PEG,BSA}$ columns represent averages across the ten simulations for each case, with standard deviations reported between parentheses.

PEG MM (kDa)	average radius of gyration (Å)			$D^{COM}_{PEG,BSA}$ (Å)	percentage of time as shroud-like conformation (%)	
	free PEG	grafted PEG	R_s		K116	N-terminal*
2	15.4 (3.1)	15.1 (3.1)	42.9 (3.1)	36.6 (9.1)	76.1	12.2
5	21.6 (4.7)	25.7 (4.7)	49.1 (6.0)	38.9 (11.3)	82.7	59.3
10	28.6 (5.0)	30.2 (7.7)	56.1 (6.3)	50.3 (12.6)	65.9	81.8
20	49.7 (7.4)	44.2 (6.7)	77.2 (8.8)	29.2 (14.2)	100	95.7

*Data taken from previous simulation work on N-terminal PEGylated BSA[33]

According to calculated $D^{COM}_{PEG,BSA}$ values in **Table 1**, it was observed that PEG chains, regardless of MM, consistently favored shroud-like conformations ($R_s > D^{COM}_{PEG,BSA}$). In 2, 5, and 10 kDa K116 PEGylated BSA, average $D^{COM}_{PEG,BSA}$ values were smaller than corresponding R_s values, suggesting partial coverage of the protein surface consistent with a transition into a shroud-like conformation. In 20 kDa K116 PEGylated BSA, the average $D^{COM}_{PEG,BSA}$ value of 29.2 Å was significantly smaller than the corresponding R_s value of 77.2 Å, suggesting more extended coverage as the polymer wrapped around the protein. The larger standard deviations for the bioconjugates are related with the broad range of initial conformations studied, where the initial structures away from domain III contributed the most (e.g. green, purple, cyan, and pink in the case of 10 kDa PEG MM - **Figure S2c**.) The fraction of time during which the PEG chain assumed a shroud-like conformation increased (76.1 to 82.7%) as the PEG chain MM increased from 2 to 5 kDa yet notably decreased (82.7 to 65.9%) in 10 kDa PEG chains before increasing again in 20 kDa PEG chains (65.9 to 100%). These results contrast with findings in our previous work on N-terminal PEGylated BSA systems, where the fraction of time during which the grafted PEG chain assumed a shroud-like conformation consistently increased as a function of PEG MM (**Table 1** and **Table S2**). In other words, a transition from the dumbbell-like to shroud-like conformation was observed in N-terminal PEGylated systems. Not only was favorability for the dumbbell-like conformation not observed in

K116 PEGylated systems, but the expected increase in affinity for the shroud-like conformation as PEG chain MM increased was also absent, as seen in the 10 kDa PEGylated system. Thus, major differences were observed in the pattern of favorability for the shroud-like conformation within 2-10 kDa PEG MM conjugates when the conjugation site was changed from the N-terminal to K116. For example, in 2 kDa K116 PEGylated BSA systems, a substantially increased percentage of time of stabilization for the shroud-like conformation was seen when compared to N-terminal PEGylated conjugates.

To explore the degree of localization of PEG with respect to the protein and the grafting site, the PEGylated BSA was approximated to mimic a system in which a spring is attached to a sphere. Hence, we measured the angle, denoted θ, between the centers of mass of the PEG chain, carbamate linker, and BSA, as illustrated in **Figure 1**. If θ tends to remain below ~90°, it indicates that the PEG chain is likely wrapping onto or collapsing toward the protein surface, promoting protein-PEG interactions. A distribution of θ markedly higher than ~90°, however, suggests the PEG chain is dangling away from the protein. The frequency distribution of θ for 2, 5, 10, and 20 kDa PEGylated conjugates with both K116 and N-terminal grafting sites was calculated and is shown in **Figure S4**. The distribution of θ in 2 kDa K116 PEGylated BSA conjugates was unexpectedly similar to that of corresponding N-terminal conjugates – an interesting result as there was considerable difference in favored conformations for the grafted 2 kDa PEG chains, with N-terminal grafted chains assuming dumbbell-like shapes while K116 grafted polymers adopted shroud-like shapes. Another noteworthy result lied in the distribution of θ for the 10 kDa K116 PEGylated BSA system in which a more uniform θ distribution was observed, suggesting markedly different dynamics of the PEG chain when compared to corresponding N-terminal PEGylated systems.

Further analysis of the K116 grafting site revealed that when the grafted PEG chain interacts with the domain I-domain III cleft, the grafted end of the polymer, rather than the free end (end of polymer which is not grafted to the protein), was dominantly interacting with the aforementioned region. For PEG repeating units near the grafted end to interact with the cavity, K116 and the carbamate linker must adopt an inward orientation – an outcome seen in all PEG MM conjugate systems (**Figure S5**). Moreover, the behavior of 2 kDa PEG polymers was seen to be more sensitive to the adopted inward orientation, due to its short length, which resulted in high-angle conformations while $D_{PEG,BSA}^{COM}$ values remained low.

The observed changes in low MM grafted PEG chain dynamics were the result of the conjugation sites' locations as these sites determine the manner in which the PEG chain can approach and form interactions with surface patches of the BSA (particularly in domain III). Therefore, the behavior of the PEG chain was evaluated with respect to the type of interaction between the protein and the polymer, which not only provides insight toward grafted PEG chain dynamics but also serves as an alternative, albeit less direct,

method of estimating PEG chain conformations. Thus, protein-PEG interactions were quantified by monitoring contacts between the BSA and the grafted PEG chain throughout the simulation time, where a contact was defined as an instance in which atoms of the BSA and the grafted polymer, excluding hydrogen atoms, were within 5 Å of each other. Specifically, we investigated how dynamics of the grafted PEG chain changed across PEG MM by measuring how long each repeating unit of the PEG chain was in contact with the protein surface for each simulation. Results are presented in **Figure 2** and colored according to the simulation's ID, referred to as sim ID (blue, red, orange, yellow, green, cyan, purple, pink, brown, and gray for sim IDs 1 through 10, respectively) — a scheme that is consistent for all results presented in this work so as to facilitate the extraction of any patterns between initial PEG conformations and consequent conjugate dynamics.

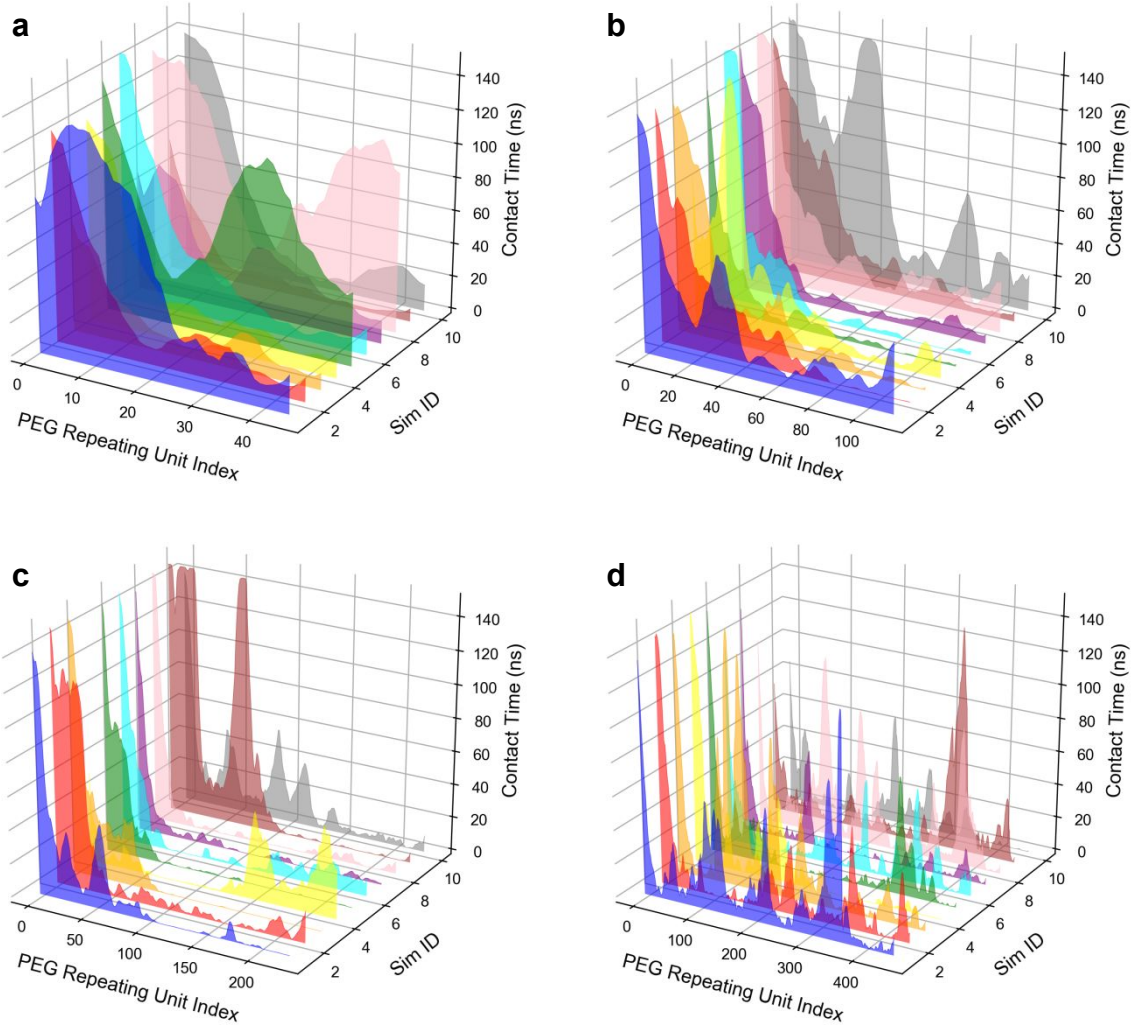

Figure 2. Contact time across repeating units of the grafted PEG polymer in 2 (a), 5 (b), 10 (c), and 20 (d) kDa K116 PEGylated BSA trajectories, where index 1 designates the repeating unit bonded to the carbamate linker. Contact time was measured for each of the ten simulations per PEG MM, referred to as "Sim ID" and colored as follows: blue, red, orange, yellow, green, cyan, purple, pink, brown, and gray.

According to **Figure 2**, high contact times were observed for the first 30-40 repeating units near the grafted end of the polymer in K116 PEGylated BSA trajectories for all PEG MM (note range changes for the "PEG repeating unit index" axes in **Figure 2a-d**), after which the PEG chain remained in solution until it reached an attractive patch on the BSA's surface. As previously mentioned, both K116 and the carbamate linker tended to orient toward the BSA's hydrophobic cavity, allowing the grafted end of the PEG chain to interact with the protein surface. The inward orientation of K116 and the carbamate linker and the resulting arrangement of preferential interactions between the grafted end of the PEG chain, which is restricted in its mobility, and the hydrophobic pocket is entropically favorable when compared to the more flexible free end of the PEG chain interacting with the pocket. An instance of this arrangement can be observed in **Figure 1**. Indeed, as PEG chain repeating units near the grafted end of the polymer were observed to significantly interact with the protein surface, the free end of the polymer, specifically in 10 kDa systems, more often dangled freely above the surface, giving rise to a wide distribution of θ values. Thus, PEG repeating units near the free end of the grafted PEG chain maintained relatively lower contact times with any region of the BSA's surface, particularly in 5 and 10 kDa K116 PEGylated systems. This indicates that while 5 and 10 kDa PEG polymers were long enough for the free end of the PEG chain to extend and interact with the protein surface, such as with patches in domain III, such conformations of PEG chain free end-BSA interaction were short lived. It is important to point out that due to the differences in the MM, the dangling free component of the polymer in 10 kDa PEG is considerably higher compared to 5 kDa PEG chains.

The nature of the observed dynamics is a consequence of the resulting entropic penalties. In an instance where the free end of the PEG chain forms preferential interactions with residue patches on the protein surface, the conformation of the PEG chain mimics a coil in which both ends are clamped. Conversely, in cases where interactions are formed predominantly by PEG repeating units near the grafting end, the resulting conformation mimics a coil clamped at only one end, allowing the other end to be mobile (**Figure S6**). In both instances, interactions may occur with the same regions of the accessible protein surface and the enthalpic gain will be similar. However, the length of the polymer and patches of the protein surface (in which the polymer is in contact with) governs which conformation is favored. In this case, we observed 5 and 10 kDa polymers to mimic a coil clamped at one end (the grafted end), leaving the free end to dangle. In this way, the effective volume that the free end may explore is significantly higher. Also, when the PEG chain behaves as a coil clamped at both ends, the excluded volume of the protein reduces the number of available conformations for the polymer and incurs an entropic penalty that cannot be avoided.

Furthermore, in the majority of trajectories for 2, 5, and 20 kDa K116 PEGylated BSA systems, appreciable contact time was not only observed for repeating units near the grafting end but in repeating units throughout the length of the polymer. In 10 kDa K116 PEGylated BSA systems, however, results from eight of the ten trajectories showed that

contact time was only prominent in the first ~110 repeating units of the grafted PEG chain, beyond which interactions were transient and minimal. Segments of high contact time in 10 kDa grafted PEG chains were approximately the length of a 5 kDa PEG polymer (113 repeating units). These findings not only support the discussed observations of 10 kDa grafted PEG chain behavior (**Figure S7**), emphasizing how the chemical environment of the conjugation site and the grafted PEG MM permits only a portion of the polymer to be able to interact with the BSA's surface while the rest protrudes away, but also provide an explanation for the presented distribution of θ in 10 kDa K116 PEGylated systems. Indeed, the dynamic portion of the polymer which was not in contact with the protein, but instead protruding away, can significantly vary the distribution of the center of mass of PEG relative to the centers of mass of the protein and linker, resulting in the observed uniform distribution of θ.

When considering similar analyses for N-terminal PEGylated BSA systems (**Figure S8**), notable differences were seen in results for 2 kDa PEGylated BSA trajectories where contact time persisted for repeating units near the grafting site followed by a steep drop along the length of the polymer. These results underline the significant deviation in 2 kDa PEG chain conformations between grafting sites as 2 kDa K116 grafted PEG chains more often assumed a shroud-like shape when compared to N-terminal grafted PEG chains. Additionally, results for 10 kDa N-terminal PEGylated BSA trajectories showed that contact times were broadly distributed throughout the entire length of the polymer when compared to K116 PEGylated systems, indicating conjugation to the protein's N-terminal does not restrict interaction between the PEG chain and the BSA in the manner observed due to the environment present near K116. Results from contact measurements, together with findings from distance and angle analyses, indicate the behavior and dynamics of lower MM PEG chains (2 to 10 kDa) are more sensitive to the effects of the grafting site.

When evaluating PEG chain conformations, the presumed behavior of the polymer as a random coil in solution draws additional consideration. While experimental determination of polymer conformation typically involves rotational averaging which yields a spherical shape of Gaussian distribution[76–79], recent research has instead emphasized the importance of the instantaneous shape of the polymer[78,80–84], which has been demonstrated to be more aspherical and anisotropic. These studies have introduced a measure of shape for flexible polymer chains that involves calculation of eigenvalues of the radius of gyration tensor.[85] The analysis leads to a visualization of the polymer as an ellipsoid. Three calculated principal moments of inertia, denoted I_x, I_y, and I_z and ordered such that $I_z > I_y > I_x$, represent major and minor axes of the ellipsoid. The ratio of the lengths of the major and minor axes (I_z/I_x and I_z/I_y), known as aspect ratios, are considered in the characterization of polymer shape. Furthermore, the relative shape anisotropy (RSA) can be calculated, which assumes a value between 0 and 1, where 0 indicates a spherical shape for the polymer and 1 suggests an ellipsoidal shape.[77] Aspect ratios and RSA values for simulations of K116 PEGylated BSA conjugates, N-terminal PEGylated BSA conjugates, and free polymers of 2, 5, 10, and 20 kDa were calculated and are

reported in **Table 2**. Results show that RSA values for grafted polymers varied between 0.09-0.14, indicating slight deviation from a spherical conformation, and aspect ratio calculations exhibited a consistent asymmetry in I_z/I_x and I_z/I_y values, underlining the shape anisotropy of the PEG polymers. Specifically, I_z/I_x aspect ratios were significantly higher than corresponding I_z/I_y aspect ratios in grafted 2, 5, 10 and 20 kDa PEG chains in both N-terminal and K116 PEGylated systems. As mentioned before, the large standard deviations are related with the broad range of initial conformations studied.

Table 2. Relative shape anisotropy (RSA) values and aspect ratios for K116 PEGylated BSA conjugates, N-terminal PEGylated BSA conjugates, and free polymers of 2, 5, 10, and 20 MMs. Values in each column represent averages across the ten simulations for each case, with standard deviations reported between parentheses.

PEG MM (kDa)	relative shape anisotropy			aspect ratio (I_z/I_x)			aspect ratio (I_z/I_y)		
	free PEG	N-terminal	K116	free PEG	N-terminal	K116	free PEG	N-terminal	K116
2	0.113 (0.049)	0.106 (0.047)	0.124 (0.045)	5.178 (3.214)	4.683 (2.742)	5.862 (3.931)	1.148 (0.123)	1.165 (0.133)	1.154 (0.135)
5	0.092 (0.047)	0.137 (0.028)	0.110 (0.036)	4.012 (2.369)	5.893 (1.966)	4.502 (1.801)	1.155 (0.112)	1.135 (0.070)	1.112 (0.072)
10	0.093 (0.040)	0.143 (0.029)	0.096 (0.034)	3.870 (1.894)	6.446 (2.701)	3.769 (1.224)	1.148 (0.111)	1.114 (0.069)	1.211 (0.119)
20	0.125 (0.040)	0.097 (0.036)	0.088 (0.028)	5.610 (3.060)	3.886 (1.566)	3.438 (0.917)	1.150 (0.125)	1.278 (0.185)	1.192 (0.091)

Structure and Dynamics of PEGylated BSA

Upon investigation of the behavior of the grafted PEG chain, in this section we evaluate the dynamics of the protein with respect to interactions with the polymer. In PEGylated proteins, there may be favorable interactions between the polymer and specific patches or domains of the protein. An understanding of these protein-PEG interactions is of great importance, specifically when one considers the shielding effect that may be imparted by the grafted PEG chain. Preferential interactions between PEG chains and key protein residues can result in shielding of binding motifs and the consequent steric hindrance can lower accessibility of substrates and reduce bioactivity. We evaluated the degree of such interactions with respect to the BSA by measuring the number of contacts per residue of the BSA over time for each K116 PEGylated BSA system. The resulting intensity map is shown in **Figure 3**, where intensity indicates the number of atoms of each residue in contact with the grafted PEG chain within 5 Å.

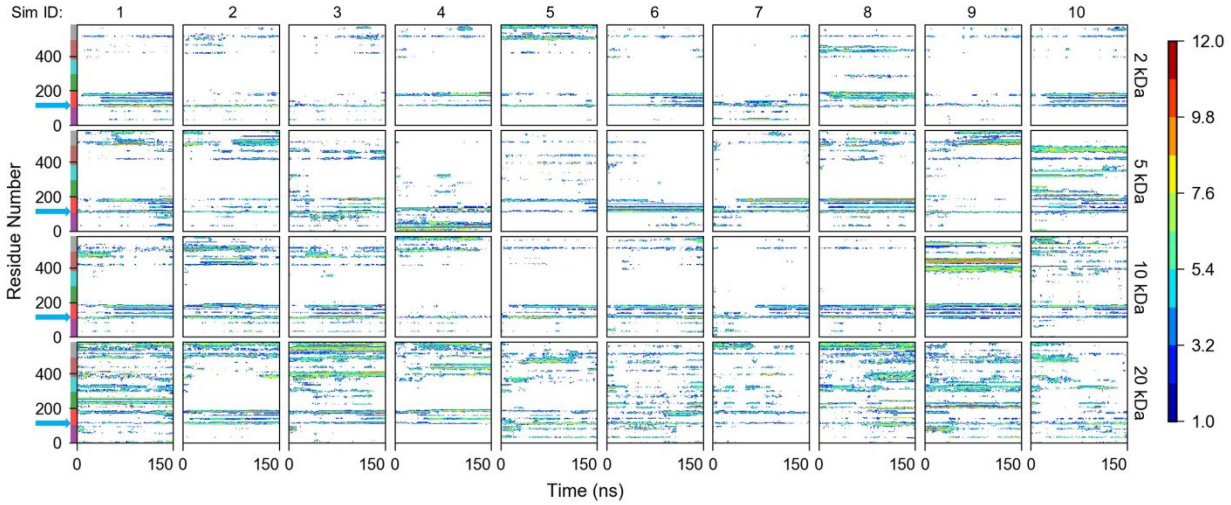

Figure 3. Intensity map for evolution of contacts in 2, 5, 10, and 20 kDa K116 PEGylated BSA trajectories, where intensity indicates the number of atoms of the residue in contact (within 5 Å) with the grafted PEG chain. Each row presents results for simulations 1 to 10 (left to right) for each MM. Color bars to the left designate the corresponding subdomain for each residue, partitioned as IA (purple), IB (red), IIA (green), IIB (cyan), IIIA (brown), and IIIB (gray). Residue K116 is identified with a cyan arrow on the left.

In the 2 kDa K116 PEGylated BSA systems (first row), significant interactions were seen in three trajectories, particularly near residue patches in domain III of the BSA; the majority of remaining trajectories showed similarly sustained protein-PEG interactions mainly localized near domain I and domain III. In contrast, interactions in 2 kDa N-terminal PEGylated BSA were limited and transient in residues not in proximity of the grafting site.[33] Interactions continued to be prevalent in 5 kDa K116 PEGylated BSA trajectories (second row) and there was an increase in contacts between residue patches in domain I of the BSA and the PEG chain. Contacts throughout 10 kDa K116 PEGylated BSA trajectories (third row) were similarly localized to domain I and III of the BSA. In 20 kDa K116 PEGylated BSA systems (fourth row), the number of residues in contact with the PEG chain expectedly increased significantly – all trajectories exhibited sustained protein-PEG interactions. Additionally, low MM PEGylated systems did not show significant interaction between domain II of the BSA and PEG, while 20 kDa systems did exhibit such contacts. It is important to highlight that each sim ID corresponds to a different initial conformation. For example, within 10 kDa PEGylated systems, contact maps (panels 5 to 8 in **Figure 3**) correspond to initial conformations colored green (in the middle), cyan, purple, and pink (to the right) in **Figure S2c**, where the initial structures of all four conformations were away from domain III. While initial orientations of PEG chains induce variance in resulting protein-PEG interactions, and must be considered in the interpretation of results, contact analysis showed that, overall, interactions were consistently more prominent in K116 PEGylated systems than in N-terminal PEGylated systems across all PEG chain MM.

Based on the identified preferential interactions between PEG and the BSA, conjugate trajectories were further investigated to discern surface patches or regions of the BSA with relatively high PEG occupancy. Scaled heatmaps of protein-PEG contact time per residue of the BSA overlaid on the three-dimensional structure of the protein (**Figure 4**) show increasing numbers of high-intensity patches as a function of PEG MM. Such residue patches were most prominent in domains I and III of the BSA; consistency of regions of high contact time between K116 and N-terminal PEGylated systems indicates that “hotspots” of PEG-BSA interaction on the BSA’s surface persist across conjugation sites and are a consequence of the protein’s geometry and surface amino acid composition. Additionally, volumetric displays of grafted PEG densities around the BSA’s surface (**Figure 4**) illustrate the most frequent three-dimensional arrangement of the polymer and increasing levels of surface coverage, particularly on domain III. These results show that such dynamics of PEG-BSA interactions, and the resulting protein surface coverage, can block accessibility of substrates to both fatty acid binding sites and Sudlow sites (found at the interface of domain I and II as well as in domain III) located near the BSA’s observed hotspots.[55,56,58] Considering the geometry of the BSA and the PEG chain MM required to preferentially interact with domain III of the protein, we predict that PEGylation of a polymer chain with MM between 5-10 kDa in a region away from these hotspots (i.e., K261) could reduce the likelihood of the polymer obscuring these domains, thus potentially retaining the bioactivity while increasing the blood circulation time due to increased radius.

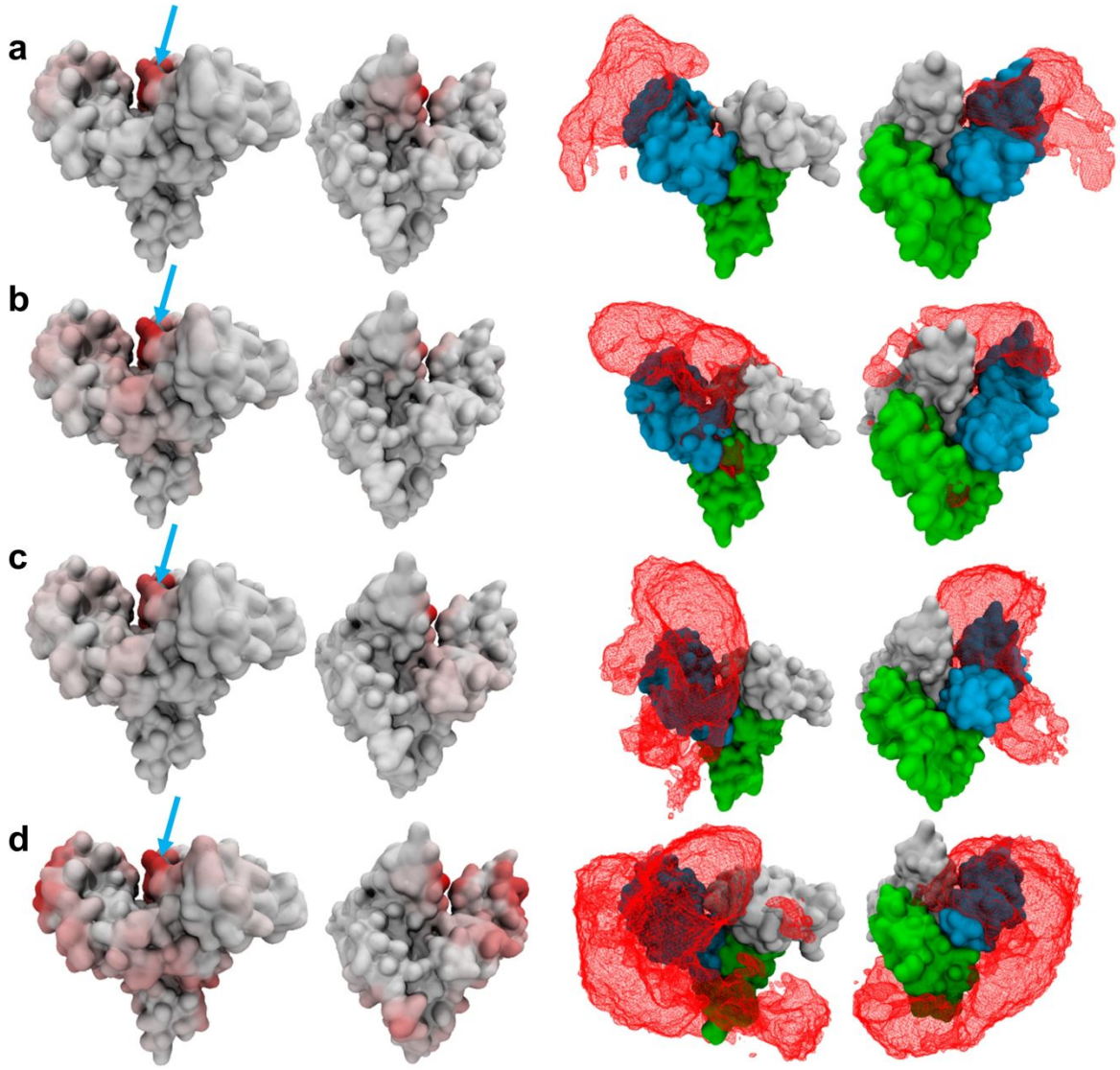

Figure 4. (left) Scaled heatmap overlaid on three-dimensional structure of the BSA in 2 (a), 5 (b), 10 (c) and 20 (d) kDa K116 PEGylated BSA conjugates. Intensity represents contact time, the time during which atoms of PEG and the BSA are within 5 Å of each other and is scaled to 0-1 as a white-red scheme where white is 0 contact time and red is 100% contact time. Residue K116 is colored cyan and identified with a cyan arrow. (right) Corresponding red transparent representations of areas in which PEG density is larger than one-tenth of the highest density, where the BSA is partitioned into domain I (gray), domain II (green), and domain III (blue). Image pairs are 180^0 rotations of each other, showing representations of the front view and the back view.

Specific protein residues involved in sustained PEG-BSA interactions were also identified. The stability of such interactions was quantified through measurement of associated residence times, defined as continuous time periods of PEG-BSA contacts. The resulting unique residues of the BSA with the top twenty maximum residence times are reported in **Table S3**. High residence time values of PEG near BSA residues were observed across all PEG MM; notably, residence times of 2 kDa K116 PEGylated systems were

comparable in magnitude to other PEG MM (~120 ns) whereas those for 2 kDa N-terminal PEGylated systems were significantly lower (~30 ns). Moreover, residence times for residues across all PEG MM systems increased for K116 PEGylated conjugates in comparison to N-terminal PEGylated conjugates, particularly for hydrophobic residues. While many residues with high maximum residence times were located within domain III of the BSA, those with hydrophobic nature were more often localized to the binding pocket of the grafting site. These observed increased residence times for hydrophobic residues in domain III and within the cavity is attributed to the surrounding chemical environment. For instance, several residues near grafting site K116, such as L115, I141, I181, L189, and A193, collectively form a hydrophobic residue patch within the cavity. Proximity of PEG to this hydrophobic patch results in favorable protein-PEG interactions with higher enthalpic gain. Additionally, there was a high frequency of lysine residues among residues with top maximum residence times, agreeing with our previous findings showing that lysine residues promote stable interactions with PEG via the PEG chain forming a looplike structure in which oxygen atoms of the polymer can form hydrogen bonds with the residue.[33]

The patterns of protein-PEG interactions observed in this work directly relate to current notions of the effect of PEGylation on protein function – the reduction of protein activity upon PEGylation is often attributed to steric hindrance on the protein's surface and obstruction of active sites resulting from contacts between the protein and polymer.[16,86,87] However, a polymer's coverage of the protein surface may not be the only mechanism of activity loss as such interactions may instead contribute to altered protein dynamics, including modified domain motions, that can more directly affect protein function. To evaluate changes and distortion to the BSA's structure upon PEGylation, preliminary analyses included calculation of root-mean-square-deviations (RMSDs) of the protein backbone as well as of each domain of the BSA (**Table S4** and **Figure S9**). Additionally, evolution of the distance between the centers of mass of each pair of domains of the BSA over time was computed and is presented in **Figure S10**. Results show that several trajectories experienced periods of higher variability in the distance between domains I and III when compared to average values calculated for the free BSA. Additionally, contact information collected from **Figure 2** and **Figure 3** indicated that the perceived domain I-domain III distance fluctuations in conjugate systems were correlated with local crowding of PEG and increased PEG-BSA interactions in domain I and III. Variations in both RMSD values and distances between centers of mass of domains were also more apparent in low MM (2 to 10 kDa) PEGylated BSA systems.

Principle component analysis (PCA) was also performed on alpha carbons in the BSA for each simulation using the ProDy python package.[73,74] Specifically, eigenvectors were extracted from the covariance matrix for Cα atoms of the BSA across all trajectories and results are presented in a scree plot (**Figure S11**), ranked in descending order of variance. An inspection of the scree plot reveals that the PEG chain had the capability to affect domain motions and the degree of such effects depended on the adopted

conformation of the grafted PEG chain. In general, it was observed that PEGylation affected low mode domain motions in the BSA, increasing their magnitude, particularly for conjugate systems in which grafted PEG chains heavily favored shroud-like conformations, when compared to molecular vibrations in the free BSA. This effect was clearly evident and more prominent in 20 kDa PEGylated systems, in which all simulations exhibited increased low mode domain motions. Observed low modes were consistent with experimentally speculated domain motions.[47,48,88]

Utilization of multiple initial conformations of PEG polymers within PEG-BSA conjugates, along with currently available experimental data, enabled us to effectively access a microsecond time scale to gain a better understanding of the effect of PEGylation towards the BSA's domain motions. This simulation study will not only assist us in understanding dynamics of PEG when grafted near a confined hydrophobic cavity, but also in designing effective drug molecules. We also note that the time scale required to achieve adequate sampling dramatically increases for high MM grafted PEG chains. To access the dynamics of extended states, and effectively calculate the free energy landscape of the vast conformational space for the protein-polymer conjugate, coarse-grained molecular dynamics[89] and enhance sampling methodologies[90] may be required.

Conclusion

In this study, atomistic molecular dynamics simulations of Lysine 116, K116, PEGylated BSA systems with 2, 5, 10, and 20 kDa molecular masses were conducted. K116's location within a hydrophobic pocket between domains I and III of the BSA provided a unique grafting environment to investigate local crowding effects. Center of mass calculations revealed that grafted PEG chains in K116 PEGylated conjugates favored shroud-like conformations, regardless of PEG molecular mass. Additionally, angle analyses and polymer contact measurements showed that the confined environment of the grafting site limited the ability of 10 kDa polymers to extend and sample the protein's surface. For 10 kDa polymers, the free polymer end dangled around the protein surface while the grafted end dominantly interacted with the protein surface – mimicking dynamics of a coil clamped in one end rather than a coil clamped in both ends.

Two reasons for increased favorability for the shroud-like conformation were identified: proximity of the grafting site (K116) toward patches of residues in domain III of the BSA and increased PEG chain affinity toward the hydrophobic cleft between domain I and domain III in the BSA. Interactions within these two regions promoted protein-PEG affinity, inducing wrapping of the polymer onto the protein surface. These results emphasized the importance in considering the effect of the conjugation site, especially for low molecular mass PEG chains, since these chains are generally observed to adopt dumbbell-like shapes, instead of the shroud-like conformations.[15,21]

Preferential interactions between the BSA and the grafted PEG chain were then explored. Contact measurements revealed regions of high contact time (hotspots) in domains I and III of the BSA. Particularly, lysine residues were found to maintain sustained protein-PEG interactions by promoting stable looplike conformations in the polymer. These observations were consistent with previous work on N-terminal PEGylated BSA conjugates, demonstrating how sustained PEG-BSA interactions were a consequence of the geometry of the protein as well as the chemical nature of the protein surface, including the relative amino acid composition. However, contact analysis revealed that 2 kDa PEG grafted at K116 had higher residence time near residues compared to what was observed when PEGylation was at the N-terminal. Considering the geometry of the BSA and the PEG chain MM required to preferentially interact with domain III of the protein, we predict that PEGylation of a polymer chain with MM between 5-10 kDa in a region away from these hotspots (i.e., K261) could reduce the likelihood of the polymer obscuring these domains, thus potentially retaining the bioactivity while increasing the blood circulation time due to increased radius.

Supporting Information

Schematic of carbamate linker; initial structures of PEGylated BSA systems; correction factor derivation for R_g and distance calculations, θ angle calculations, snapshots of K116 and linker orientations, snapshots of polymer grafted end and free end interactions, snapshots of 5 kDa and 10 kDa grafted polymer conformations, contact time for grafted polymers in N-terminal PEGylated BSA systems, evolution of RMSD over time calculations for the BSA protein backbone in PEGylated systems, evolution of distance between centers of mass of domains I & II, domains I & III, and domains II & III of the BSA in PEGylated systems, PCA analysis scree plot, visualization of first three low mode vibrations of the BSA, simulation system sizes for all PEGylated conjugates, R_g and distance calculations for N-terminal PEGylated BSA systems, top residence times for residues of the BSA in PEGylated systems, average RMSD values for the protein backbone and each domain of the BSA in PEGylated systems.

Acknowledgments

The authors acknowledge the computational support provided by University of Florida Research Computing, which contributed to the results reported in this publication.

Funding Sources

Financial assistance provided by the University of Florida Preeminence Initiative and the US National Science Foundation, SI2 program, Grant: 1613155.

References

1 B. Leader, Q. J. Baca and D. E. Golan, Protein therapeutics: a summary and pharmacological classification, *Nat. Rev. Drug Discov.*, 2008, **7**, 21–39.

2 P. Carter, Introduction to current and future protein therapeutics: a protein engineering perspective, *Exp. Cell Res.*, 2011, **317**, 1261–1269.

3 H. A. D. Lagassé, A. Alexaki, V. L. Simhadri, N. H. Katagiri, W. Jankowski, Z. E. Sauna and C. Kimchi-Sarfaty, Recent advances in (therapeutic protein) drug development, *F1000Research*, 2017, **6**, 113–130.

4 R. Duncan, The dawning era of polymer therapeutics, *Nat. Rev. Drug Discov.*, 2003, **2**, 347–360.

5 H. Maeda, SMANCS and polymer-conjugated macromolecular drugs: advantages in cancer chemotherapy, *Adv Drug Deliv Rev.*, 2001, **46**, 169–185.

6 R. Haag and F. Kratz, Polymer therapeutics: concepts and applications, *Angew Chem Int Ed Engl.*, 2006, **45**, 1198–1215.

7 A. Abuchowski, T. van Es, N. C. Palczuk and F. F. Davis, Alteration of immunological properties of bovine serum albumin by covalent attachment of polyethylene glycol, *J. Biol. Chem.*, 1977, **252**, 3578–3581.

8 F. M. Veronese and A. Mero, The Impact of PEGylation on Biological Therapies, *BioDrugs*, 2008, **22**, 315–329.

9 M. Swierczewska, K. C. Lee and S. Lee, What is the future of PEGylated therapies?, *Expert Opin. Emerg. Drugs*, 2015, **20**, 531–536.

10 J. Israelachvili, The different faces of poly(ethylene glycol), *Proc. Natl. Acad. Sci. U. S. A.*, 1997, **94**, 8378–8379.

11 J. M. Harris and R. B. Chess, Effect of pegylation on pharmaceuticals, *Nat. Rev. Drug Discov.*, 2003, **2**, 214–221.

12 M. L. Nucci, R. Shorr and A. Abuchowski, The therapeutic value of poly(ethylene glycol)-modified proteins, *Adv. Drug Deliv. Rev.*, 1991, **6**, 133–151.

13 R. B. Greenwald, Y. H. Choe, J. McGuire and C. D. Conover, Effective drug delivery by PEGylated drug conjugates, *Adv. Drug Deliv. Rev.*, 2003, **55**, 217–250.

14 D. Li, B. N. Manjula and A. S. Acharya, Extension Arm Facilitated PEGylation of Hemoglobin: Correlation of the Properties with the Extent of PEGylation, *Protein J.*, 2006, **25**, 263–274.

15 R. Ferebee, I. F. Hakem, A. Koch, M. Chen, Y. Wu, D. Loh, D. C. Wilson, J. L. Poole, J. P. Walker, G. Fytas and M. R. Bockstaller, Light Scattering Analysis of Mono- and Multi-PEGylated Bovine Serum Albumin in Solution: Role of Composition on Structure and Interactions, *J. Phys. Chem. B*, 2016, **120**, 4591–4599.

16 B. Plesner, C. J. Free, P. Westh and A. D. Nielsen, Effects of PEG size on structure, function and stability of PEGylated BSA, *Eur. J. Pharm. Biopharm.*, 2011, **79**, 399–405.

17 Y. R. Gokarn, M. McLean and T. M. Laue, Effect of PEGylation on Protein Hydrodynamics, *Mol. Pharm.*, 2012, **9**, 762–773.

18 A. Basu, K. Yang, M. Wang, S. Liu, R. Chintala, T. Palm, H. Zhao, P. Peng, D. Wu, Z. Zhang, J. Hua, M.-C. Hsieh, J. Zhou, G. Petti, X. Li, A. Janjua, M. Mendez, J. Liu, C. Longley, Z. Zhang, M. Mehlig, V. Borowski, M. Viswanathan and D.

Filpula, Structure−Function Engineering of Interferon-β-1b for Improving Stability, Solubility, Potency, Immunogenicity, and Pharmacokinetic Properties by Site-Selective Mono-PEGylation, *Bioconjug. Chem.*, 2006, **17**, 618–630.

19 L. He, H. Wang, V. M. Garamus, T. Hanley, M. Lensch, H.-J. Gabius, C. J. Fee and A. Middelberg, Analysis of MonoPEGylated Human Galectin-2 by Small-Angle X-ray and Neutron Scattering: Concentration Dependence of PEG Conformation in the Conjugate, *Biomacromolecules*, 2010, **11**, 3504–3510.

20 C. J. Fee and J. M. Van Alstine, Prediction of the Viscosity Radius and the Size Exclusion Chromatography Behavior of PEGylated Proteins, *Bioconjug. Chem.*, 2004, **15**, 1304–1313.

21 C. Le Cœur, S. Combet, G. Carrot, P. Busch, J. Teixeira and S. Longeville, Conformation of the Poly(ethylene Glycol) Chains in DiPEGylated Hemoglobin Specifically Probed by SANS: Correlation with PEG Length and in Vivo Efficiency, *Langmuir*, 2015, **31**, 8402–8410.

22 S. S. Pai, B. Hammouda, K. Hong, D. C. Pozzo, T. M. Przybycien and R. D. Tilton, The Conformation of the Poly(ethylene glycol) Chain in Mono-PEGylated Lysozyme and Mono-PEGylated Human Growth Hormone, *Bioconjug. Chem.*, 2011, **22**, 2317–2323.

23 E. Vernet, G. Popa, I. Pozdnyakova, J. E. Rasmussen, H. Grohganz, L. Giehm, M. H. Jensen, H. Wang, B. Plesner, H. M. Nielsen, K. J. Jensen, J. Berthelsen, M. Sundström and M. van de Weert, Large-Scale Biophysical Evaluation of Protein PEGylation Effects: In Vitro Properties of 61 Protein Entities, *Mol. Pharm.*, 2016, **13**, 1587–1598.

24 D. I. Svergun, F. Ekström, K. D. Vandegriff, A. Malavalli, D. A. Baker, C. Nilsson and R. M. Winslow, Solution structure of poly(ethylene) glycol-conjugated hemoglobin revealed by small-angle x-ray scattering: Implications for a new oxygen therapeutic, *Biophys. J.*, 2008, **94**, 173–181.

25 G. Cattani, L. Vogeley and P. B. Crowley, Structure of a PEGylated protein reveals a highly porous double-helical assembly, , DOI:10.1038/NCHEM.2342.

26 C. Yang, D. Lu and Z. Liu, How PEGylation Enhances the Stability and Potency of Insulin: A Molecular Dynamics Simulation, *Biochemistry*, 2011, **50**, 2585–2593.

27 Q. Mu, T. Hu and J. Yu, Molecular Insight into the Steric Shielding Effect of PEG on the Conjugated Staphylokinase: Biochemical Characterization and Molecular Dynamics Simulation, *PLoS One*, 2013, **8**, e68559.

28 K. Ciepluch, A. Radulescu, I. Hoffmann, A. Raba, J. Allgaier, D. Richter and R. Biehl, Influence of PEGylation on Domain Dynamics of Phosphoglycerate Kinase: PEG Acts Like Entropic Spring for the Protein, *Bioconjug. Chem.*, 2018, **29**, 1950–1960.

29 G. Settanni, J. Zhou and F. Schmid, Interactions between proteins and poly(ethylene-glycol) investigated using molecular dynamics simulations, *J. Phys. Conf. Ser.*, 2017, **921**, 012002.

30 D. Xu, N. Smolin, R. K. Shaw, S. R. Battey, A. Tao, Y. Huang, S. E. Rahman and M. L. Caylor, Molecular insights into the improved clinical performance of PEGylated interferon therapeutics: a molecular dynamics perspective, *RSC Adv.*, 2018, **8**, 2315–2322.

31 B. N. Manjula, A. Tsai, R. Upadhya, K. Perumalsamy, P. K. Smith, A. Malavalli, K.

Vandegriff, R. M. Winslow, M. Intaglietta, M. Prabhakaran, J. M. Friedman and A. S. Acharya, Site-Specific PEGylation of Hemoglobin at Cys-93(β): Correlation between the Colligative Properties of the PEGylated Protein and the Length of the Conjugated PEG Chain, *Bioconjug. Chem.*, 2003, **14**, 464–472.

32 B. Khameneh, M. R. Jaafari, M. Hassanzadeh-Khayyat, A. Varasteh, J. Chamani, M. Iranshahi, H. Mohammadpanah, K. Abnous and M. R. Saberi, Preparation, characterization and molecular modeling of PEGylated human growth hormone with agonist activity, *Int. J. Biol. Macromol.*, 2015, **80**, 400–409.

33 A. Munasinghe, A. Mathavan, A. Mathavan, P. Lin and C. M. Colina, Molecular Insight into the Protein–Polymer Interactions in N-Terminal PEGylated Bovine Serum Albumin, *J. Phys. Chem. B*, 2019, **123**, 5196–5205.

34 A. M. Merlot, D. S. Kalinowski and D. R. Richardson, Unraveling the mysteries of serum albumin-more than just a serum protein, *Front. Physiol.*, 2014, **5**, 299.

35 E. L. Gelamo and M. Tabak, Spectroscopic studies on the interaction of bovine (BSA) and human (HSA) serum albumins with ionic surfactants, *Spectrochim. Acta Part A Mol. Biomol. Spectrosc.*, 2000, **56**, 2255–2271.

36 Z. Liu and X. Chen, Simple bioconjugate chemistry serves great clinical advances: albumin as a versatile platform for diagnosis and precision therapy, *Chem. Soc. Rev.*, 2016, **45**, 1432–1456.

37 M. M. Castellanos and C. M. Colina, Molecular Dynamics Simulations of Human Serum Albumin and Role of Disulfide Bonds, *J. Phys. Chem. B*, 2013, **117**, 11895–11905.

38 R. K. Sahu, P. Nacharaju, B. N. Manjula and S. A. Acharya, Induced Plasma Expander-like Properties as a Function of PEG-chains on Extension Arm Facilitated PEGylation of Albumin: “Mushroom to Brush-Like” Conformational Transition of the PEG-albumin Conjugate, *Artif. Cells, Blood Substitutes, Biotechnol.*, 2009, **37**, 245–256.

39 J. Dozier and M. Distefano, Site-Specific PEGylation of Therapeutic Proteins, *Int. J. Mol. Sci.*, 2015, **16**, 25831–25864.

40 T. H. Kim, H. H. Jiang, S. M. Lim, Y. S. Youn, K. Y. Choi, S. Lee, X. Chen, Y. Byun and K. C. Lee, Site-Specific PEGylated Exendin-4 Modified with a High Molecular Weight Trimeric PEG Reduces Steric Hindrance and Increases Type 2 Antidiabetic Therapeutic Effects, *Bioconjug. Chem.*, 2012, **23**, 2214–2220.

41 J. Xu, J. Bussiere, J. Yie, A. Sickmier, P. An, E. Belouski, S. Stanislaus and K. W. Walker, Polyethylene Glycol Modified FGF21 Engineered to Maximize Potency and Minimize Vacuole Formation, *Bioconjug. Chem.*, 2013, **24**, 915–925.

42 M. Danial, T. H. H. van Dulmen, J. Aleksandrowicz, A. J. G. Pötgens and H.-A. Klok, Site-Specific PEGylation of HR2 Peptides: Effects of PEG Conjugation Position and Chain Length on HIV-1 Membrane Fusion Inhibition and Proteolytic Degradation, *Bioconjug. Chem.*, 2012, **23**, 1648–1660.

43 K. O. Ramberg, P. M. Antonik, D. L. Cheung and P. B. Crowley, Measuring the Impact of PEGylation on a Protein–Polysaccharide Interaction, *Bioconjug. Chem.*, 2019, **30**, 1162–1168.

44 C. S. Cazalis, C. A. Haller, L. Sease-Cargo and E. L. Chaikof, C-Terminal Site-Specific PEGylation of a Truncated Thrombomodulin Mutant with Retention of Full Bioactivity, *Bioconjug. Chem.*, 2004, **15**, 1005–1009.

45 Y. Tsutsumi, M. Onda, S. Nagata, B. Lee, R. J. Kreitman and I. Pastan, Site-specific chemical modification with polyethylene glycol of recombinant immunotoxin anti-Tac(Fv)-PE38 (LMB-2) improves antitumor activity and reduces animal toxicity and immunogenicity, *Proc. Natl. Acad. Sci. U. S. A.*, 2000, **97**, 8548–8553.
46 C. T. Kuan, Q. C. Wang and I. Pastan, Pseudomonas exotoxin A mutants. Replacement of surface exposed residues in domain II with cysteine residues that can be modified with polyethylene glycol in a site-specific manner., *J. Biol. Chem.*, 1994, **269**, 7610–7616.
47 S. Fujiwara and T. Amisaki, Molecular dynamics study of conformational changes in human serum albumin by binding of fatty acids, *Proteins Struct. Funct. Bioinforma.*, 2006, **64**, 730–739.
48 S. Biswas and P. K. Chowdhury, Correlated and Anticorrelated Domain Movement of Human Serum Albumin: A Peek into the Complexity of the Crowded Milieu, *J. Phys. Chem. B*, 2016, **120**, 4897–4911.
49 A. H. Elcock, Models of macromolecular crowding effects and the need for quantitative comparisons with experiment, *Curr. Opin. Struct. Biol.*, 2010, **20**, 196–206.
50 H.-X. Zhou, G. Rivas and A. P. Minton, Macromolecular crowding and confinement: biochemical, biophysical, and potential physiological consequences, *Annu. Rev. Biophys.*, 2008, **37**, 375–397.
51 A. Zaghmi, E. Mendez-Villuendas, A. A. Greschner, J. Y. Liu, H. W. de Haan and M. A. Gauthier, Mechanisms of activity loss for a multi-PEGylated protein by experiment and simulation, *Mater. Today Chem.*, 2019, **12**, 121–131.
52 A. M. Alkilany, S. Mansour, H. M. Amro, B. Pelaz, M. G. Soliman, J. G. Hinman, J. M. Dennison, W. J. Parak and C. J. Murphy, Introducing Students to Surface Modification and Phase Transfer of Nanoparticles with a Laboratory Experiment, *J. Chem. Educ.*, 2017, **94**, 769–774.
53 J. M. Harris, N. H. Hundley, T. G. Shannon and E. C. Struck, Polyethylene glycols as soluble, recoverable, phase-transfer catalysts, *J. Org. Chem.*, 1982, **47**, 4789–4791.
54 G. E. Totten and N. A. Clinton, Poly(ethylene Glycol) and Derivatives as Phase Transfer Catalysts, *J. Macromol. Sci. Part C*, 1998, **38**, 77–142.
55 G. Sudlow, D. J. Birkett and D. N. Wade, The Characterization of Two Specific Drug Binding Sites on Human Serum Albumin, *Mol. Pharmacol.*, 1975, **11**, 824–832.
56 G. Sudlow, D. J. Birkett and D. N. Wade, Further Characterization of Specific Drug Binding Sites on Human Serum Albumin, *Mol. Pharmacol.*, 1976, **12**, 1052–1061.
57 J. C. Phillips, R. Braun, W. Wang, J. Gumbart, E. Tajkhorshid, E. Villa, C. Chipot, R. D. Skeel, L. Kalé and K. Schulten, Scalable molecular dynamics with NAMD, *J. Comput. Chem.*, 2005, **26**, 1781–1802.
58 A. Bujacz, Structures of bovine, equine and leporine serum albumin, *Acta Crystallogr. Sect. D Biol. Crystallogr.*, 2012, **68**, 1278–1289.
59 J. M. Word, S. C. Lovell, J. S. Richardson and D. C. Richardson, Asparagine and glutamine: using hydrogen atom contacts in the choice of side-chain amide

orientation 1 1Edited by J. Thornton, *J. Mol. Biol.*, 1999, **285**, 1735–1747.
60 M. E. Fortunato and C. M. Colina, pysimm : A python package for simulation of molecular systems, *SoftwareX*, 2017, **6**, 7–12.
61 J. K. Dozier and M. D. Distefano, Site-Specific PEGylation of Therapeutic Proteins., *Int. J. Mol. Sci.*, 2015, **16**, 25831–64.
62 J. Huang, S. Rauscher, G. Nawrocki, T. Ran, M. Feig, B. L. de Groot, H. Grubmüller and A. D. MacKerell Jr, CHARMM36m: an improved force field for folded and intrinsically disordered proteins, *Nat. Methods*, 2017, **14**, 71–73.
63 C. G. Mayne, J. Saam, K. Schulten, E. Tajkhorshid and J. C. Gumbart, Rapid parameterization of small molecules using the Force Field Toolkit, *J. Comput. Chem.*, 2013, **34**, 2757–2770.
64 K. Vanommeslaeghe, E. Hatcher, C. Acharya, S. Kundu, S. Zhong, J. Shim, E. Darian, O. Guvench, P. Lopes, I. Vorobyov and A. D. Mackerell Jr, CHARMM general force field: A force field for drug-like molecules compatible with the CHARMM all-atom additive biological force fields, *J. Comput. Chem.*, 2010, **31**, 671–690.
65 K. Vanommeslaeghe and A. D. MacKerell Jr., Automation of the CHARMM General Force Field (CGenFF) I: bond perception and atom typing, *J. Chem. Inf. Model*, 2012, **52**, 3144–3154.
66 K. Vanommeslaeghe, E. P. Raman and A. D. MacKerell Jr., Automation of the CHARMM General Force Field (CGenFF) II: Assignment of bonded parameters and partial atomic charges, *J. Chem. Inf. Model*, 2012, **52**, 3155–3168.
67 W. Humphrey, A. Dalke and K. Schulten, VMD: Visual molecular dynamics, *J. Mol. Graph.*, 1996, **14**, 33–38.
68 A. Mathavan, A. Mathavan, M. Fortunato and C. M. Colina, An All-Atomistic Molecular Dynamics Study to Determine the Structural Importance of Disulfide Bonds in Immunoglobulin G and Bovine Serum Albumin, *AJUR*, 2018, **15**, 6–22.
69 W. L. Jorgensen, J. Chandrasekhar, J. D. Madura, R. W. Impey and M. L. Klein, Comparison of simple potential functions for simulating liquid water, *J. Chem. Phys.*, 1983, **79**, 926.
70 M. W. Mahoney and W. L. Jorgensen, A five-site model liquid water and the reproduction of the density anomaly by rigid, non-polarizable models, *J. Chem. Phys.*, 2000, **112**, 8910–8922.
71 T. Darden, D. York and L. Pedersen, Particle mesh ewald: An N ·log(N) method for ewald sums in large systems, *J. Chem. Phys.*, 1993, **98**, 10089–10092.
72 S. Miyamoto and P. A. Kollman, SETTLE: An analytical version of the SHAKE and RATTLE algorithm for rigid water molecules, *J. Comput. Chem.*, 1992, **13**, 952–962.
73 A. Bakan, L. M. Meireles and I. Bahar, ProDy: Protein Dynamics Inferred from Theory and Experiments, *Bioinformatics*, 2011, **27**, 1575–1577.
74 A. Bakan, A. Dutta, W. Mao, Y. Liu, C. Chennubhotla, T. R. Lezon and I. Bahar, Evol and ProDy for bridging protein sequence evolution and structural dynamics, *Bioinformatics*, 2014, **30**, 2681–2683.
75 J. R. Molek and A. L. Zydney, Ultrafiltration characteristics of pegylated proteins, *Biotechnol. Bioeng.*, 2006, **95**, 474–482.
76 P. Debye and F. Bueche, Distribution of Segments in a Coiling Polymer Molecule,

J. Chem. Phys., 1952, **20**, 1337–1338.
77 D. N. Theodorou and U. W. Suter, Shape of unperturbed linear polymers: polypropylene, *Macromolecules*, 1985, **18**, 1206–1214.
78 C. Haber, S. A. Ruiz and D. Wirtz, Shape anisotropy of a single random-walk polymer, *Proc. Natl. Acad. Sci.*, 2000, **97**, 10792–10795.
79 M. Triantafillou and R. D. Kamien, Polymer shape anisotropy and the depletion interaction, *Phys. Rev. E*, 1999, **59**, 5621–5624.
80 W. Khun and H. Khun, Rigidity of chain molecules and its determination from viscosity and flow birefringence in dilute solutions, *J. Colloid Sci.*, 1948, **3**, 11–32.
81 H. Lee, R. M. Venable, A. D. MacKerell and R. W. Pastor, Molecular Dynamics Studies of Polyethylene Oxide and Polyethylene Glycol: Hydrodynamic Radius and Shape Anisotropy, *Biophys. J.*, 2008, **95**, 1590–1599.
82 H. Lee, A. H. de Vries, S.-J. Marrink and R. W. Pastor, A Coarse-Grained Model for Polyethylene Oxide and Polyethylene Glycol: Conformation and Hydrodynamics, *J. Phys. Chem. B*, 2009, **113**, 13186–13194.
83 B. H. Zimm, Chain Molecule Hydrodynamics by the Monte-Carlo Method and the Validity of the Kirkwood-Riseman Approximation, *Macromolecules*, 1980, **13**, 592–602.
84 K. A. Rubinson and S. Krueger, Poly(ethylene glycol)s 2000–8000 in water may be planar: A small-angle neutron scattering (SANS) structure study, *Polymer (Guildf).*, 2009, **50**, 4852–24858.
85 K. Šolc, Shape of a Random-Flight Chain, *J. Chem. Phys.*, 1971, **55**, 335–344.
86 B. Unterweger, T. Stoisser, S. Leitgeb, R. Birner-Grünberger and B. Nidetzky, Engineering of Aerococcus viridansl-Lactate Oxidase for Site-Specific PEGylation: Characterization and Selective Bioorthogonal Modification of a S218C Mutant, *Bioconjug. Chem.*, 2012, **23**, 1406–1414.
87 Y.-S. Wang, S. Youngster, M. Grace, J. Bausch, R. Bordens and D. F. Wyss, Structural and biological characterization of pegylated recombinant interferon alpha-2b and its therapeutic implications, *Adv. Drug Deliv. Rev.*, 2002, **54**, 547–570.
88 F. Ameseder, R. Biehl, O. Holderer, D. Richter and A. M. Stadler, Localised contacts lead to nanosecond hinge motions in dimeric bovine serum albumin, *Phys. Chem. Chem. Phys.*, 2019, **21**, 18477–18485.
89 F. Ramezanghorbani, P. Lin and C. M. Colina, Optimizing Protein–Polymer Interactions in a Poly(ethylene glycol) Coarse-Grained Model, *J. Phys. Chem. B*, 2018, **122**, 7997–8005.
90 A. Bhattarai and Y. Miao, Gaussian accelerated molecular dynamics for elucidation of drug pathways, *Expert Opin. Drug Discov.*, 2018, **13**, 1055–1065.

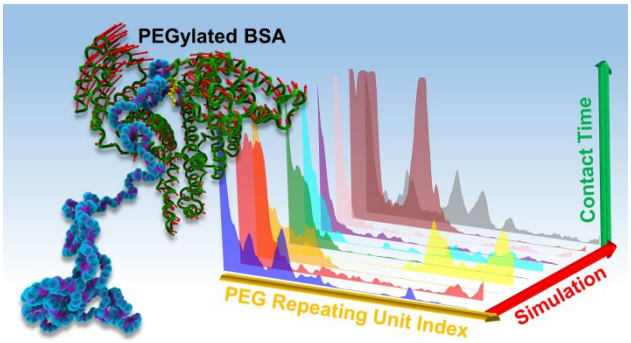
PEGylated BSA
Contact Time
Simulation
PEG Repeating Unit Index